Dynamic Modeling of a Solar Receiver/Thermal Energy Storage System Based on a Compartmented Dense Gas Fluidized Bed

Roberto Solimene[1, a)], Roberto Chirone[2, b)], Riccardo Chirone[1] and Piero Salatino[2]

1 Istituto di Ricerche sulla Combustione, Consiglio Nazionale delle Ricerche, Piazzale Vincenzo Tecchio 80, 80125 Napoli (Italy)
2 Dipartimento di Ingegneria Chimica, dei Materiali e della Produzione Industriale, Università degli Studi di Napoli Federico II, Piazzale Vincenzo Tecchio 80, 80125 Napoli (Italy)

[a)]Corresponding author: solimene@irc.cnr.it
[b)]roberto.chirone.13@ucl.ac.uk present position: PhD student at University College of London, London, United Kingdom

Abstract. Fluidized beds may be considered a promising option to collection and storage of thermal energy of solar radiation in Concentrated Solar Power (CSP) systems thanks to their excellent thermal properties in terms of bed-to-wall heat transfer coefficient and thermal diffusivity and to the possibility to operate at much higher temperature. A novel concept of solar receiver for combined heat and power (CHP) generation consisting of a compartmented dense gas fluidized bed has been proposed to effectively accomplish three complementary tasks: collection of incident solar radiation, heat transfer to the working fluid of the thermodynamic cycle and thermal energy storage. A dynamical model of the system laid the basis for optimizing collection of incident radiative power, heat transfer to the steam cycle, storage of energy as sensible heat of bed solids providing the ground for the basic design of a 700kW_{th} demonstration CSP plant.

INTRODUCTION

Development and deployment of Concentrated Solar Power (CSP) generation is gaining renewed interest. The US Department of Energy has launched the SunShot program [1] targeted at reducing the LCOE from CSP to less than 6cent/kWh. The European Commission has laid the path to CSP development and deployment in the Framework Programs and in the forthcoming SET plan [2]. A survey by IEA has recently analyzed priorities and opportunities associated with CSP [3], highlighting the key role of integrated thermal energy storage (TES) and fuel-power hybridization for the successful exploitation of concentrated solar power.

Dense gas-solid fluidized suspensions are proposed as heat transfer fluid (HTF) [4-8] thanks to their excellent thermal properties in terms of bed-to-wall heat transfer coefficient and thermal diffusivity [9-11]. Moreover they can be used as effective thermal energy storage media. The use of fluidized solids as alternative to other storage/exchange media, like molten salts, entails the possibility to overcome issues associated with the use of corrosive or environmentally unfriendly fluids. No less importantly, the system can be operated at much higher temperature under direct irradiation of solid particles [12-15]. Dense gas-solid fluidized beds have the potential to effectively accomplish three complementary tasks: a) the collection of incident solar radiation; b) the transfer of the incident power to heat exchange surfaces and henceforth to high-efficiency steam and/or organic Rankine cycles; c) thermal energy storage, aimed at equalizing the inherent time-variability of the incident radiation for stationary CHP generation. All these features have been exploited in a novel concept of solar receiver for CHP generation with thermal energy storage. The concept is based on a novel design of the solar collector, consisting of a compartmented dense gas fluidized bed capable of performing the three complementary tasks (collection, storage and transfer) [8]. Non-conventional design

and operation of fluidized beds based on uneven or unsteady (pulsed) fluidization [7,16], may further enhance their thermal performances for CSP applications.

A dynamical model of the compartmented solar receiver is hereby presented. Computations are aimed at optimizing specific features of the solar generation unit (SGU), with a focus on the accomplishment of the three basic tasks by a compartmented design of the fluidized bed unit and a tailored control strategy.

THE MODEL

The Solar Receiver for CHP Generation

The basic concept is the development of a SGU consisting of a compartmented dense gas fluidized bed, Fig. 1(a), optimized so as to accomplish the following three complementary tasks: collection, storage and transfer of solar energy, while keeping constant the firm capacity load.

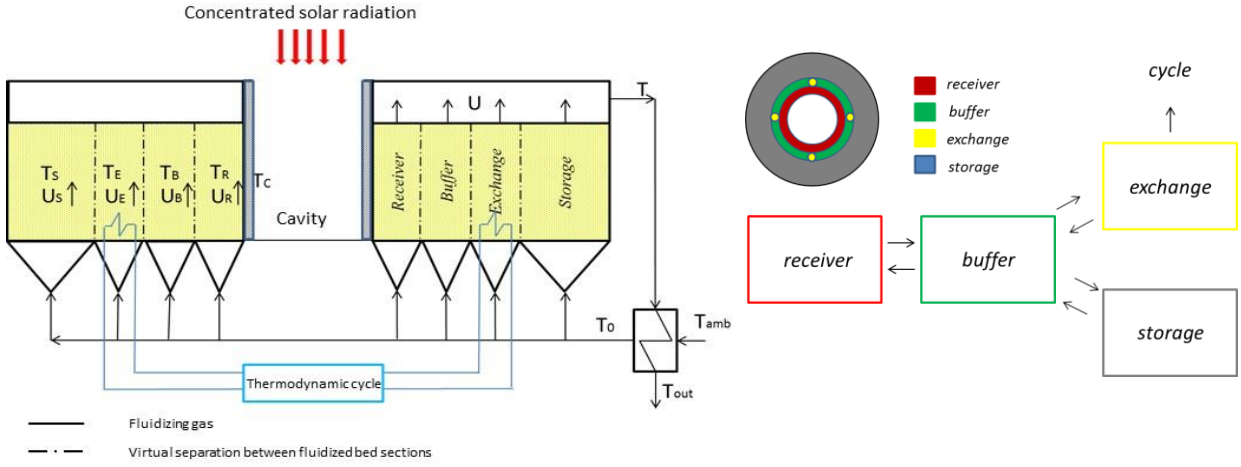

(a) (b)

FIGURE 1. Conceptual representation of the solar receiver/thermal energy storage system based on compartmented dense gas fluidized beds (a); Schematic views of RES/RSE configuration of the SGU and of heat fluxes (b).

The concept is based on the inherently properties of dense fluidized beds of featuring: large bed-to-surface heat transfer coefficients, which can be tuned by acting on the fluidization parameters and large effective thermal diffusivities, associated with convective transfer due to bubble-induced and gulfstream motion of fluidized solids. Both features may be optimized by proper selection of fluidized solids type and size and fluidization regime.

The system consists of a cylindrical cavity, where the incident solar radiation is concentrated by the heliostat field and the secondary reflector, a bubbling gas fluidized bed coupled with a steam cycle and an external heat exchanger for partial recovery of the enthalpy of the effluent gas. The windbox is compartmented so as to achieve independent control of fluidization in each of the different zones: 1) the receiver section (R), located nearby the cavity; 2) the exchange section (E), where heat exchange surfaces are immersed; 3) an auxiliary buffer section (B); 4) the storage section (S), aimed at thermal energy storage as sensible heat of the fluidized solids. The incident power is transferred serially from the receiver section to the buffer section, which further distributes the power between the exchange and the storage sections.

It is important to underline that the four zones are not physically separated but they are obtained by a not uniform feed of fluidizing gas. Different feasible configurations have been studied. The most promising solution Fig. 1(b), named RES/RSE configuration, is characterized by a central receiver section and the exchange section made by four heat exchangers immersed in the buffer section. This configuration ensures that all the different sections are in contact according to a series-parallel schema (Fig. 1(b)).

The Control Strategy

The control strategy developed in this paper is finalized to obtain the operative conditions of the plant able to provide a constant thermal load for a pre-set time interval. The incident solar power varies during the day, so, to prevent that the output load follows the same trend, it is necessary the presence of a thermal storage section and that the power output is lower than the solar peak thermal load during the pre-set time interval, Δt. The starting time t_1 is arbitrarily pre-set, whereas t_2 is associated with the features of the storage section which provides a constant by means of the energy stored during the diurnal phase. In particular, the scope is to provide a stable thermal power output transferred to the exchange section during the time interval Δt to have a very small rangeability for the power cycle. A key role in the control logic is played by the "Buffer" section (B) whose task is to regulate the energy flows. The ambition of the control strategy is to keep the exchange section temperature at values close to the temperature of set-point T_{ES} during the energy production phase. Outside the time interval, Δt, the exchange section is defluidized and the energy flows from or to the exchange sections are stopped. During the energy production phase, two stages can be considered: an "active phase" and a "passive phase". During the "active phase" the temperature of the buffer section is higher than the temperature of the storage section, $T_B > T_S$. This is typical of diurnal phases of greater insolation. In this case the surplus of the incident power compared to the "firm capacity load" is send to the storage section. On the other side during the "passive phase" the temperature of the buffer section is lower than the temperature of the storage section, $T_B < T_S$. This is typical of the evening and of the night. In this case the deficit of incident power compared to the "firm capacity load" is compensated by the energy accumulated in the storage section. The control dynamically acts on the fluidization velocity of the different bed sections in order to control heat transfer between different zones of the bed and to limit heat losses associated to enthalpy of the gasses leaving the system.

Model Equations

The mathematical model is based on the three-dimensional configuration arrangement reported in Fig. 1. The model is based on the following assumptions:

1. The incident solar radiation is uniformly dispersed over the lateral surface of the cavity;
2. The wall between the cavity and the fluidized bed is modeled by lumped parameter so the temperature is uniform throughout its volume;
3. The view factor F_c is only a function of geometric parameters of the cavity;
4. The natural-convection heat transfer of the cavity is modeled through a constant pre-set coefficient h_{cn};
5. The transient behavior of the air-air heat recuperator is neglected by assuming pseudo steady state conditions considering that the thermal transient of the recuperator is faster than that of the receiver;
6. The two different phases in the fluidized bed are modeled as a single phase with average properties assuming thermal equilibrium between the bed solids and the fluidizing gas;
7. Gas heat capacity in granular bed is negligible compared to the heat capacity of bed solids;
8. Pseudo steady state behavior is considered for the freeboard being its thermal dynamics faster than that of the fluidized bed;
9. Abrasion and elutriation phenomena are negligible: the fluidized bed mass can be considered constant;
10. The heat flows through the different sections of the bed are modeled according to the Fourier law;
11. The virtual separation of the bed is considered equivalent to a physical separation;
12. Each bed section behaves as a perfect insulator with respect to the others and to the cavity under fixed bed conditions;
13. The fluidized bed is lumped into four zones (R, B, E and S), within which the solid and gas phases are well stirred. It is assumed that the use of a compartmented windbox provides an effective way to independently control fluidization conditions in each zone without having physical separtions between the four zones
14. Heat transfer coefficient, h_{bed}, between the fluidized bed and immersed surfaces is calculated according to Molerus et al. [17].

Heat transfer flux exchanged between the i-th and j-th fluidized bed sections is proportional to their temperature difference by means of a transfer coefficient $k_{i,j}$ given by the following equation:

$$k_{i,j} = \rho_s cp_s (1 - \varepsilon_{mf}) \frac{\alpha_{i,j}}{\delta_{i,j}} \quad (1)$$

where ρ_s, cp_s, ε_{mf}, and $\delta_{i,j}$ are bed solids density and specific heat capacity, the bed voidage at incipient fluidization and the length scale of heat transfer based on the geometrical features of the i-th and j-th fluidized bed sections,

respectively. The effective thermal diffusivity, $\alpha_{i,j}$, averaged between the i-th and j-th fluidized bed sections is dominated by convection of fluidized solids and has been expressed according to Borodulya et al. [18].

The model equations consist of the transient energy balance on the cavity, the transient energy balances on R, B, E and S sections of the fluidized bed, the energy balance at the fluidized bed exhaust, the energy balances on air-air heat recovery exchanger and are reported by means of the following eqns. 2-9.

$$m_c \cdot c_c \frac{dT_c}{dt} = [1-(1-e_w)\cdot F_c]\cdot Q_{in}(t) - \left[h_{bed}\cdot(T_c - T_R)\cdot S_l + h_{cn}\cdot(T_c - T_{amb}) + F_c \cdot e_w \cdot \sigma \cdot {T_c}^4\right] \quad (2)$$

$$m_R \cdot cp_s \frac{dT_R}{dt} = h_{bed}\cdot(T_c - T_R)\cdot S_l - k_{R,B}\cdot S_{R,B}\cdot(T_R - T_B) - S_R \cdot U_R \cdot \rho_{air}(T_R)\cdot cp_{air}\cdot(T_R - T_0) \quad (3)$$

$$m_B \cdot cp_s \frac{dT_B}{dt} = k_{E,B}\cdot S_{E,B}\cdot(T_E - T_B) + k_{R,B}\cdot S_{R,B}\cdot(T_R - T_B) + k_{S,B}\cdot S_{S,B}\cdot(T_S - T_B) - S_B \cdot U_B \cdot \rho_{air}(T_S)\cdot cp_{air}\cdot(T_B - T_0) \quad (4)$$

$$m_E \cdot cp_s \frac{dT_E}{dt} = k_{B,E}\cdot S_{B,E}\cdot(T_B - T_E) - \left(\frac{S_f}{\frac{1}{h_{bed}}+\frac{1}{h_f}}\right)\cdot(T_E - T_f) + S_E \cdot U_E \cdot \rho_{air}(T_E)\cdot cp_{air}\cdot(T_E - T_0) \quad (5)$$

$$m_S \cdot cp_s \frac{dT_S}{dt} = k_{E,S}\cdot S_{E,S}\cdot(T_E - T_S) + k_{B,S}\cdot S_{B,S}\cdot(T_B - T_S) - S_S \cdot U_S \cdot \rho_{air}(T_S)\cdot cp_{air}\cdot(T_S - T_0) \quad (6)$$

$$S_R \cdot U_R \cdot \rho_{air}(T_R)\cdot cp_{air}\cdot T_R + S_B \cdot U_B \cdot \rho_{air}(T_B)\cdot cp_{air}\cdot T_B + S_E \cdot U_E \cdot \rho_{air}(T_E)\cdot cp_{air}\cdot T_E + S_S \cdot U_S \cdot \rho_{air}(T_S)\cdot cp_{air}\cdot T_S = \begin{pmatrix} S_R \cdot U_R \cdot \rho_{air}(T_R) + S_E \cdot U_E \cdot \rho_{air}(T_E) + \\ + S_S \cdot U_S \cdot \rho_{air}(T_S) + S_B \cdot U_B \cdot \rho_{air}(T_B) \end{pmatrix}\cdot cp_{air}\cdot T \quad (7)$$

$$\dot{M}\cdot cp_{air}(T - T_{out}) = \dot{M}\cdot cp_{air}(T_0 - T_{amb}) \quad (8)$$

$$\dot{M}\cdot cp_{air}(T_0 - T_{amb}) = U_{EX}\cdot S(T - T_0) \quad (9)$$

where m_c, c_c , T_c , e_w , F_c and S_l are the mass, specific heat, temperature, emissivity, view factor and area of the lateral surface of the cavity. $Q_{in}(t)$ is the incident radiative solar power which is described by a sine function during the diurnal phase and is 0 during the night. h_{nc} and σ are the heat transfer coefficient due to natural convection in the cavity and the Stefan-Boltzmann constant. m_i, T_i, S_i and U_i are mass, temperature, cross section and fluidization velocity of the i-th fluidized bed section. $\rho_{air}$and cp_{air} are the density and specific heat of air. S_f, h_f and T_f are the heat transfer surface, the fluid-side heat transfer coefficient in the exchange section and the working fluid temperature, respectively. T_0, T, T_{out} and T_{amb} are the temperatures of the gas at inlet and outlet of the fluidized bed, the temperature of the effluent gas, the ambient temperature. $\dot{M}$ is the mass flow rate of fluidizing gas. U_{EX} and S_{EX} are the overall heat transfer coefficient and transfer surface of air-air heat exchanger. Finally, the right-hand second term of the balance on the exchange section (eqn. 5) expresses the thermal power transferred to the thermodynamic cycle.

The control acts on the system modifying its natural evolution to get the desired behavior having two main goals: i) to limit the heat losses; ii) to keep, during the time interval, Δt, the thermal energy transferred to the thermodynamic cycle for the power generation almost constant. The control of receiver section is such that this section is fluidized during the insolation hours at a velocity which ensures the maximum bed-to-wall heat transfer coefficient and it is defluidized during the night hours to limit the heat losses from the bed toward the cavity. This is considered in the model by multiplying the transient energy balance of receiver section and all the receiver velocity terms U_R by the Heaviside function $g_r(t)$ which is 1 during the diurnal phase and 0 during the night. The exchange section control aims at fluidizing this section only during the time interval, Δt, during which the thermodynamic cycle is active. In this way it is able to mismatch the production of electrical energy with respect to solar radiation. To this end, the transient energy balance of exchange section and all the exchange velocity terms U_E are multiplied by the Heaviside function $h(t)$ which is 1 only in the time interval $[t_1, t_2]$. The buffer section plays a key role in the control strategy being the distribution joint of energy flows. The control is based on a Heaviside function $j_b(t)$, which multiplies the transient energy balance of buffer section and all the buffer velocity terms U_B. This function is able to fluidize the buffer section in the diurnal phase and during the night phase only if the thermodynamic cycle is working. The control action in the storage section is finalized to keep nearly contant the thermal outlet load with a low rangeabilty during the selected time interval Δt. Accordingly, this means to keep the exchange section temperature T_E approximately constant to a set-point temperature, T_{sp}, through the eqn. 10:

$$f_r(T_E, T_B, T_S) = \left[\phi(T_B - T_S)\cdot\left[\phi(T_E - T_{SP} - \Delta T_{max}) + \phi[\Delta T_{max} - (T_E - T_{SP})]\cdot\frac{T_E - T_{SP}}{\Delta T_{max}}\right]\cdot\phi(T_E - T_{SP})\right] + \left[\phi(T_S - T_B)\cdot\left[\phi(T_{SP} - T_E - \Delta T_{max}) + \phi[\Delta T_{max} - (T_{SP} - T_E)]\cdot\frac{T_{SP} - T_E}{\Delta T_{max}}\right]\cdot\phi(T_{SP} - T_E)\right] \quad (10)$$

This equation is composed by two macro-terms identifying the active phase ($T_B > T_S$) and the passive phase ($T_S > T_B$) and it multiplies the transient energy balance of storage section and all the storage velocity terms U_S. During the

active phase, the second term is 0 and, when $T_E > T_{sp}$, the storage section will be fluidized at the maximum gas velocity only when the temperature between the exchange section and the set-point is larger than a pre-set ΔT_{max}, otherwise the storage gas velocity will vary according to a linear function of the temperature difference $T_E - T_{SP}$. During the passive phase, the first term is 0 and, when $T_{sp} - T_E > \Delta T_{max}$, the storage section will be fluidized at the maximum gas velocity to bring back the exchange temperature to the set-point temperature, otherwise the storage gas velocity will vary according to a linear function of the temperature difference $T_{SP} - T_E$.

Model equations are a system of five ODEs, solved in the MathCad™ environment by a fourth order Runge–Kutta algorithm with adaptive integration step size.

Geometric properties of the plant, model parameters and values of input variables are listed in Table 1.

TABLE 1. Geometric properties of the industrial plant and model parameters.

Fluidized bed	External diameter, D_e m	10	Storage section	Storage cross section area, S_s m^2	28.4
	Bed height, H_{bed} m	2.8		Solids inventory, kg	204200
	Total cross section area, S_{tot} (m^2)	44.6	Bed solids (sand)	Density, kg/m^3	2600
Cavity	Cavity diameter, D_c m	2.7		Sauter mean diameter, μm	150
	Mass, kg	800		Voidage at incipient fluidization, -	0.45
	Irradiated surface, m^2	23.8	Steam cycle	Average T_f, K	623
	Emissivity, -	0.92		S_f, m^2	22
	View Factor, -	0.13		h_f, W/m^2K	1750
	h_{nc}, W/m^2K	5		T_{SP}, K	823
Receiver section	Receiver cross section area, S_r m^2	5.0	External heat recuperator	S_{EX}, m^2	86
	Solids inventory, kg	20100		U_{EX}, W/m^2K	50
Exchanger section	Exchange cross section area, S_e m^2	2.2	Buffer section	buffer cross section area, S_s m^2	9
	Solids inventory, kg	8900		Solids inventory, kg	58310

The incident radiative solar power concentrated into the cavity, averaged on daily base (24h), is a design variable taken for the industrial-scale plant design and fixed to 707 kW. The diurnal phase (τ_d=14.5h) and night phase (9.5h) are those typical of Sicily summer. The heat exchange toward the thermodynamic cycle is active after 7h from the sunrise and for a time interval Δt equal to 7h.The numerical solution of the differential equations allows getting the time resolved profiles of the temperature of the wall of the cavity (T_C) and of the different sections of the bed: receiver (T_R), buffer (T_B), exchange (T_E) and storage (T_S). Simulations have been performed in order to achieve the steady state conditions of the SGU which are, however, characterized by time-variability of temperatures due to the variation of the incident solar power with time and to the control stategy. As a consequence, all the thermal fluxes of the SGU were calculated on the basis of the computed time series of SGU temepratures and were averaged on daily base (24h) in order to calculate the fludized bed, the cavity and the overall thermal efficiencies of the plant according to the following equations:

$$\eta_{bed} = \frac{Q_{bed} - Q_{gas}}{Q_{bed}} \tag{11}$$

$$\eta_{cavity} = \frac{Q_{bed}}{Q_{in}} = \frac{Q_{in} - Q_{rad} - Q_{ref} - Q_{cn}}{Q_{in}} \tag{12}$$

$$\eta_{overall} = \frac{Q_{cycle}}{Q_{in}} = \frac{Q_{in} - Q_{rad} - Q_{ref} - Q_{cn} - Q_{gas}}{Q_{in}} \tag{13}$$

where Q_{bed}, Q_{gas}, Q_{in}, Q_{rad}, Q_{ref}, Q_{cn}, Q_{cycle}, are the thermal power transferred from the cavity to the receiver section, the thermal energy lost as gas entalpy leaving the system, incident solar energy, thermal radiation energy, reflected solar energy and natural convection energy lost from the cavity and the energy transferred to thermodynamic cycle.

Three different cases have been considered:

- **Case A (even and steady fluidization)**. The fluidized bed has been operated without partitioning of the fluidizing gas at fluidization velocity of 0.033 m/s, value averaged of the compartmented case B.
- **Case B (uneven and steady fluidization)**. A non-controlled compartmented case in which the R, B, E and S sections have been fluidized independently each other. The gas superficial velocity has been set at 0.02 m/s in the S and B sections. The gas superficial velocity in the R and E sections has both been set at 0.1 m/s which provides locally optimal values to maximize heat transfer with the cavity and the tube bundle, respectively.
- **Case C (uneven and controlled fluidization)**. Similar to the previous case B but with the additional implementation of the control strategy.

RESULTS AND DISCUSSION

Results of simulations are presented in Fig. 2 and in table 2 for the three different cases under investigation. Figures 2 reports the time series of the temperatures of the various sections of the SGU together with the time-resolved profile of the incident solar power for two consecutive days (48h) once the steady state conditions were reached. The temperature of 583K was arbitrarily set as initial condition for all the sections of the SGU in all the cases investigated. The steady state conditions are not dependent on the initial conditions and they are achieved when the values of variables (temperatures) averaged on daily (24h) base can be considered constant (variation less than 1%).

Analysis of case A (Fig. 2A) suggests that the temperatures of the four sections of the fluidized bed (R, B, E and S) are remarkably overlapped with each other except when the heat transfer to the thermodynamic cycle is active.

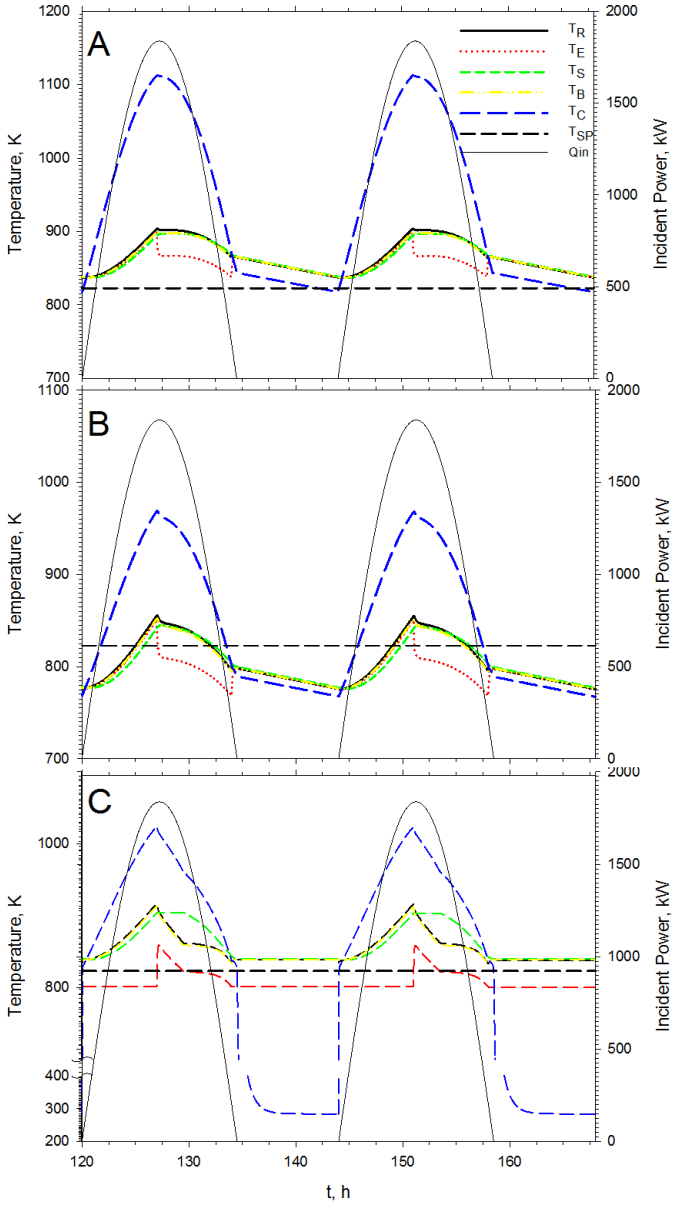

FIGURE 2. Time series of cavity and bed temperature for two consecutive days under steady state conditions together with the incident solar power. A) non-controlled and non-compartmented fludized bed; B) compartmented and non-controlled fluidized bed; C) compartmented and controlled fluidized bed.

This is a demonstration of the outstanding ability of fluidized beds to equalize bed solids temperature as a consequence of its very large effective thermal diffusivity. This finding further supports the concept of using fluid beds as effective thermal storage media. The temperature of the cavity exceeds that of the bed by nearly 100K during the active daytime phase of the cycle, to drop below it during the passive nighttime phase. The solids inventory in the bed, and the associated overall heat capacity, are such that the bed temperature never drops below the set point temperature T_{sp} over the whole period of 7h when the steam cycle is active. This might not hold true if the bed inventory, and in particular the inventory of the storage section, is reduced.

The results reported in figure 2B correspond to the compartmented case B and show that the time series of the temperatures of various sections are similar to the case A. However, some differences are evident: i) the SGU temperatures are lower of about 50K than those of case A, mainly due to higher heat transfer coefficient in the receiver and exchange sections being the gas superficial velocity larger (0.1m/s); ii) during the daytime and before the start-up of the thermodynamic cycle, storage section temperature is significantly lower than the other temperatures because of a lower gas velocity and so of a lower thermal diffusion; iii) exchange section temperature is lower than the T_{sp}, instead the temperatures of the other sections, initially higher, become lower than T_{sp} during the night.

Figure 2C highlights the effect on the time-temperature history of the unit if the control strategy is also implemented according to Case C. The defluidization of the receiver section during the passive nighttime phase causes the rapid cooling down of the cavity with a positive influence on reduction of heat losses towards the environment. The temperature of the exchange section is initially constant being defluidized, then it runs up when the thermodynamic cycle is started and the exchange section is fluidized according to control strategy. This increase of temperature is due to the heat accumulated in the receiver and buffer section and transferred to exchange section thanks to the higher thermal diffusivity when this section is fluidized. It should be noted that at this time the system evolves naturally because $T_S > T_B$ and $T_E > T_{sp}$ and the storage section remains defluidized. When the thermal energy coming from receiver and buffer section as well as from the incident solar radiation vanishes, T_E decreases and becomes lower than the set-point value. Under these conditions the fludization velocity in storage section begins to increase according to the control strategy in order to keep the exchange section temperature constant and equal to the set-point value. The exchange section temperature is almost constant for three hours then it decreases even if the storage section is fluidized at the maximum fluididization velocity.

The effect of the combination of compartmented operation of the fluidized bed and of the implementation of the control strategy is better appreciated from the table 2 which reports selected variables averaged on daily (24h) base under steady state conditions for the three cases under investigation. The averaged incident solar power is balanced by: a) thermal losses from the cavity, which, in turn, include reflection of incident radiation and radiative and natural convection losses; b) losses of sensible heat associated with the effluent gases; c) power transferred to the steam cycle. All the relevant terms in the time-averaged energy balance are reported in table 2, together with the computed overall thermal efficiency, expressed as the ratio between the power transferred to the steam cycle and the incident radiative power. The overall thermal efficiency equals the product of the cavity efficiency (accounting for cavity losses) and of the fluidized bed efficiency (accounting for losses of sensible heat of the fluidizing gas). These values are also reported in table 2 to better appreciate the relevant sources of heat losses toward the environment.

TABLE 2. Numerical results of the simulations.

Case	Power, kW						Efficiency, -		
	Incident radiation	Reflected radiation	Fluidizing gas losses	Cavity radiative losses	Cavity natural convection losses	Power to steam cycle	Cavity	Fluidized bed	overall
A	707	7.5	99	150	79	370	0.66	0.79	0.52
B	707	7.5	81	89	70	462	0.78	0.85	0.65
C	707	7.5	36	78	47	540	0.81	0.94	0.76

Comparison of the computed results for Cases A, B and C indicates the extensive improvements that can be accomplished by proper operation of the fluidized bed receiver. Optimizing the local gas superficial velocities in a compartmented bed (Case B) results in a nearly 90kW additional thermal input to the cycle mainly due to reduced cavity losses. Further improvement is accomplished in Case C by implementing an optimal control strategy: an additional thermal input to the cycle of nearly 80kW is achieved, thanks to reductions of heat losses due to fluidizing gas and from the cavity.

CONCLUSIONS

A novel concept of Concentrated Solar Power (CSP) generation system featuring thermal energy storage has been presented, based on a compartmented dense gas fluidized bed unit. A dynamical model of the system has been developed also implementing a tailored control strategy. Its implementation plays a key role to set up the operative conditions of the plant able to provide a constant thermal load for a pre-set time interval. It has been shown how model computations may be directed to optimize the operation of the system, by fully exploiting the properties of the dense fluidized bed and the opportunities given by a compartmented arrangement and a tailored control strategy. The model suggests that both the compartmentation and the control strategy may improve the performances of the SGU in terms of both energy transfer (increase of about 170kW) to the thermodynamic cycle and unit thermal efficiency (increase from 0.52 to 0.76). The mathematical model can be also use to further optimization of the system by means of full and optimal exploitation of all the input variables of the SGU.

ACKNOWLEDGMENTS

The research leading to these results has received funding from the European Union Seventh Framework Programme FP7/2007-2013 under grant agreement n° 609837, STAGE-STE project and from MIUR in the framework of the project "PON01_00761: Solare Termodinamico con Accumulo Solido (SOLTESS)" of the Program PON Ricerca e Competitività 2007-2013.

REFERENCES

1. www.solar.energy.gov/sunshot/csp.html.
2. Concentrating Solar Power – From research to implementation, European Commission (2007) ISBN 978-92-79-05355-9.
3. Technology Roadmap - Concentrating Solar Power, OECD/IEA, (2010).
4. C. K. Ho and B. D. Iverson, Renew. Sust. Energ. Rev. **29,** 835–846 (2014).
5. H. Benoit, I. Pérez López, D. Gauthier, J.-L. Sans and G. Flamant, Sol. Energy **118**, 622–633 (2015).
6. H. Benoit, L. Spreafico, D. Gauthier, and G. Flamant, Renew. Sust. Energ. Rev. **55**, 298–315 (2016).
7. P. Salatino, P. Ammendola, P. Bareschino, R. Chirone and R. Solimene, Powder Technol. **290**, 97–101 (2016).
8. R. Chirone, P. Salatino, P. Ammendola, R. Solimene, M. Magaldi, R. Sorrenti, G. De Michele and F. Donatini, "Development of a Novel Concept of Solar Receiver/Thermal Energy Storage System Based on Compartmented Dense Gas Fluidized Beds" in "The 14th International Conference on Fluidization – From Fundamentals to Products", edited by J.A.M. Kuipers, R.F. Mudde, J.R. van Ommen, N.G. Deen, ECI Symposium Series, (2013). http://dc.engconfintl.org/fluidization_xiv/123
9. E. Sette, D. Pallarès and F. Johnsson, Experimental Powder Technol. **263**, 74–80 (2014).
10. F. Niklasson, H. Thunman, F. Johnsson and B. Leckner, Ind. Eng. Chem. Res. **41**, 4663–4673 (2002).
11. F. Berruti, D. S. Scott and E. Rhodes, Can. J. Chem. Eng. **64**, 48–56 (1986).
12. G. Flamant, AIChE J **28**, 529–535 (1982).
13. D. M. Bachovchin, D. H. Archer and D. H. Neale, AIChE Symp. Ser. **79**, 27–36 (1983).
14. E. Alonso and M. Romero, Renew. Sust. Energ. Rev. **41**, 53–67 (2015).
15. C. Tregambi, R. Chirone, F. Montagnaro, P. Salatino and R. Solimene, Sol. Energy **129**, 85–100 (2016).
16. S. Migliozzi, A. Paulillo, R. Chirone, P. Salatino and R. Solimene, Powder Technol. In Press, http://dx.doi.org/10.1016/j.powtec.2016.12.052.
17. O. Molerus, A. Burschka and S. Dietz., Chem. Eng. Sci. **50**, 879–885 (1995).
18. V. A. Borodulya, Y. G. Epanov and Y. S. Teplitskii, J. Eng. Phys. **42**, 528–533 (1982).